Influence of surface topography and wettability in the boiling mechanisms

A. S. Moita*1, E. Teodori[1,2], A. L. N. Moreira[1]
*1: Instituto Superior Técnico, TU Lisbon, Av. Rovisco Pais, 1049-001 Lisbon, Portugal.
2: Universitá di Roma "Tor Vergata", Dep. Mech. Engineering, Via del Politecnico 1-00133, Rome, Italy.

Abstract

The present paper addresses the detailed analysis of the physical processes involved in pool boiling, in the context of micro-cooling applications. The results clearly show the vital effect of wettability and of the surface topography on the boiling morphology, and consequently on the heat transfer mechanisms. Hence, liquids with low surface tension will completely wet all the surfaces, delaying the triggering of nucleation. For these wetting conditions, increasing the latent heat of evaporation will require larger superheat to start the incipient boiling. Also, small increase of the surface tension and/or of the latent heat of evaporation leads to significantly different bubble dynamics. An enhancement of the heat transfer is achieved with micro-textured surfaces, within the roughness scales used here, by controlling the bubble dynamics with the rough cavities. For partially wetting liquids, having larger surface tension (*e.g.* water) the relation between the roughness amplitude *h* and the distance between the cavities λ_R has a strong effect in the coalescence of vapor bubbles, so that critical ratios h/λ_R promote the entrapment of a vapor blanket, which acts as an insulator, leading to the decrease of the heat transfer coefficient.

Introduction

Challenges arising from smaller chips, higher operating frequency in the electronic industry and brighter optical devices are leading to higher thermal loads, which cannot be addressed with conventional fin-fan cooling. Thermal loads as high as 100 W/cm^2 have been reported for various electronic devices [1,2]. In order to meet these thermal loads, boiling heat transfer is considered as an attractive option. Both pool and flow boiling are very effective in achieving high heat fluxes for a small temperature difference between the heated surface and the cooling fluid. However, maximizing the boiling heat flux in order to develop an effective cooling system is not a trivial task, given the high non-linearity of the various transport processes involved, which are intricately coupled. The boiling heat flux is affected by numerous variables such as the bubble size and departure frequency, the nucleation site density, the wall superheat, the wetting properties and the surface topography. Although the boiling phenomenon has been studied for many decades, from the early work of Lord Rayleigh [3], who derived the first expression for the inertially controlled growth or collapse of vapor bubbles and later from Nukiyama [4], who identified different boiling regimes, research work is still required to obtain an accurate model of nucleate pool boiling, research work is still required to obtain an accurate model of nucleate pool boiling. Moreover, the effect of surface roughness is sparsely understood and it has not been accurately quantified, even if it has been long known to have a significant impact on the boiling process. Jacob [5] noticed that the roughness, the level of corrosion and oxidation of the surface dramatically influence the boiling curve. During the 1950's, one of the prevailing theories was that bubbles were mostly generated from cavities containing entrapped vapor, as illustrated by Westwater [6]. This mechanism was further sustained by the experimental study of Clark *et al.* [7] and by the theoretical analysis of Bankoff [8], who confirmed the vapor entrapment theory showing that only unwetted cavities can serve as nucleation sites, while only cavities with certain shapes can serve as vapor traps. The role of the rough cavities was further addressed by Griffith and Wallis [9], who showed that the cavity radius determines the superheat required for bubble nucleation in a uniformly superheated liquid, with larger cavities requiring lower wall superheats. Hsu [10] extended this analysis to include the effects of the thermal boundary layer and showed that only a certain range of cavity sizes can serve as active nucleation sites.

The effect of surface topography on the boiling mechanisms is strongly dependent on the wetting behaviour: pool boiling of complete wetting liquids such as R-113, diethyl ether, and n-penthane was studied by Corty and Foust [11] who found that the surface roughness not only affected the superheat required for incipience but also the slope of the boiling curve. Rougher surfaces resulted in lower superheats for a given heat flux, which was attributed to the presence of larger unwetted cavities on the rougher surfaces. Similar conclusions were later reported by Kurihara and Myers [12], Hsu and Schmidt [13], Marto and Rohsenow [14] and Berenson [15], who actually report an increment of the heat transfer coefficient in 600% by roughening the heating surface. The in-

*Corresponding author: anamoita@dem.ist.utl.pt

creased understanding of the role of surface condition has also led to the development of commercially available enhanced surfaces for improved boiling performance. Many of these boiling enhancements are designed to create re-entrant-type cavity structures which are more difficult for the liquid to fully wet than simple cavity shapes and, based on the analysis of Griffith and Wallis [9], are believed to serve as more stable nucleation sites. Following this trend, much of the literature has concentrated on boiling from either smooth surfaces or those with geometrically idealized cavities such as v-shaped grooves, conical pits, or reentrant cavities. In this context, three recent works worth to be referred. Yu *et al.* [16], studied the boiling performance and flow mechanisms on artificial cylindrical micro-cavity surfaces in silicon surfaces with different geometric parameters and the characteristics. Nitesh *et al*. [17] analyzed the effect of nucleation site spacing on the pool boiling of FC72 on a silicon surface structured with pyramidal shaped re-entrant cavities. The authors suggest that there is an optimum inter-cavity spacing for which most of the surface remains active for a wide range of heat fluxes. Finally, Hutter *et al.* [18] investigated the boiling of FC 72 on a silicon chip with artificial cylindrical cavities.

Apart from a few studies, such as Hutter *et al* [18], bubble nucleation characteristics have not been the subject of many detailed studies on rough surfaces, particularly those with random roughness profiles, especially where high nucleation site densities occur. In Dhir *et al.* [19] and Zhang and Shoji [20], only groups of two to five interacting bubble sites, isolated from other sites on the surface by design, were observed or simulated for the sake of simplicity of the model.

Recently, Kotthoff and Gorenflo [21] studied the effects of surface roughness and tube diameter on nucleation site density and heat transfer coefficient in the pool boiling of various refrigerants and organic liquids from copper tubes. The authors confirmed that active site densities integrated over time are higher than those apparent over only a few ebullition periods, in agreement with the previous observations reported by Gorenflo *et al.*[22]. Based on the surface characterization performed by Luke[23], Kotthoff and Gorenflo [21] concluded that surface roughness descriptions solely based on roughness amplitude parameters (e.g. mean surface roughness R_a) cannot be used to accurately predict the influence of surface roughness so it is necessary to explore additional quantities. Similar argument has been recently presented by Moita and Moreira [24].

Jones *et al.* [25] and McHale and Garimella [26] have performed an extensive study of the pool boiling mechanisms onto rough surfaces, including the effect of roughness topography on bubble dynamics and report that bubble diameter at the departure increased with increasing wall superheat, but also suggests that this result depends on the effect of the roughness on bubble dynamics. These results could not be accurately predicted by any of the correlations considered from the literature, highlighting the need of further investigations in this field, particularly to understand the relation between the surface topography and the bubble dynamics.

In line with this, the present work addresses a detailed description of the bubble dynamics and heat transfer mechanisms occurring in pool boiling, within millimetric and micrometric scales. Different liquids are used to account for the liquid properties, as well as to infer on the additional effects of wettability in the observed phenomena. Particular emphasis is given to the influence of the surface topography, which will be mostly investigated using patterned surfaces. This analysis is expected to deepen the understanding of the pool and flow boiling phenomena occurring at the microscale, since, despite the dramatic evolution of the available diagnostic techniques, the characterization of the phenomena occurring near the wall is still very limited. Consequently, many questions remain to answer, regarding the real differences existing between the phenomena occurring at different scales.

Materials and Methodologies

The experimental setup, which is schematically represented in Figure 1, mainly consists on a power supply, a heating block, a pool boiling test section, two synchronized high-speed cameras (a Kodak Motion Corder Analyzer, Series SR 512x420pixels, Model PS-120, with a maximum frame rate of 10kfps and a Phantom v4.2 from Vision Research Inc., with 512x512pixels@2100fps and a maximum frame rate of 90kfps) and a temperature acquisition system.

Different pool boiling sections were used to infer on the effect of their dimensions in the observed phenomena. The largest section has an area of 18.75 cm^2 while the smallest has an area of 3.62 cm^2. The height varies between 15mm and 3mm. For the range considered here, any significant influence was observed by changing the section area of the pool. The test pool sections are made of glass (supported by an aluminum structure) to allow optical access from various angles.

Two different configurations were used to heat the pool film. The first consists on using a glass surface coated with a transparent film of Indium Oxide (In_2O_3), which is heated by Joule effect. Deposition of the film is made by radio frequency (rf) plasma enhanced reactive thermal evaporation (rf-PERTE) at low substrate temperature (<100ºC). This configuration is used to obtain simultaneous visualization of both side and bottom planes of the pool, which allow performing a detailed description of the mechanisms of bubble formation and departure. In the later configuration, a copper support, heated by electric cartridge heaters, is used instead, to achieve higher

heat thermal power. Figures 2 and 3 show the detailed schematic of the copper block and a global view of the test pool boiling section, respectively.

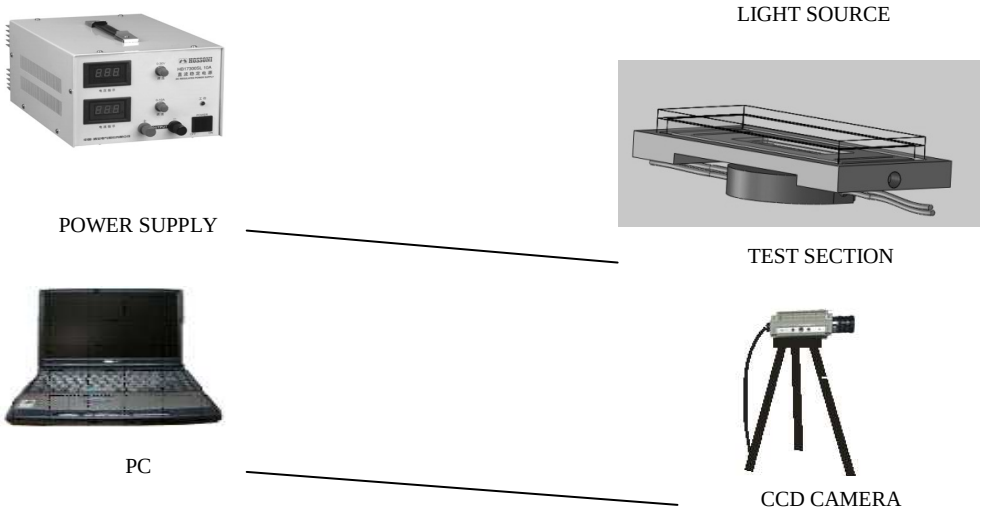

Figure 1. Schematic layout of the experimental arrangement.

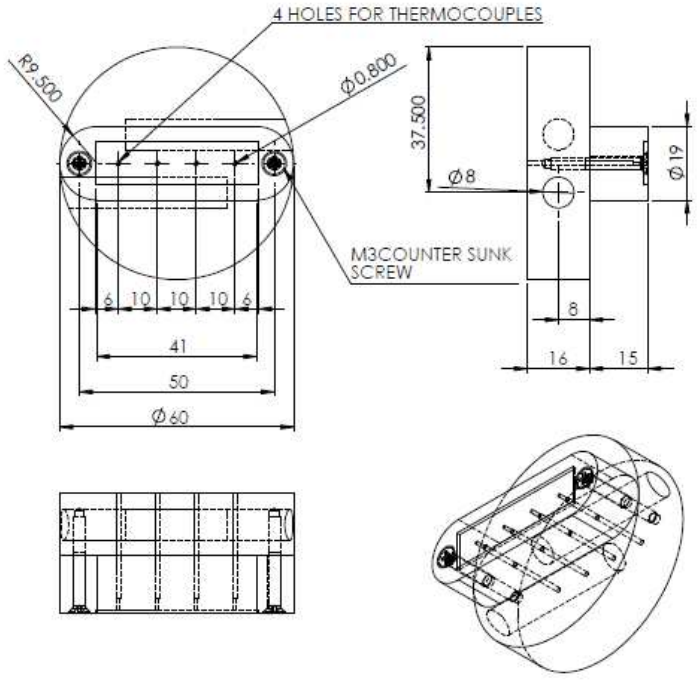

Figure 2. Detailed schematic of the copper support.

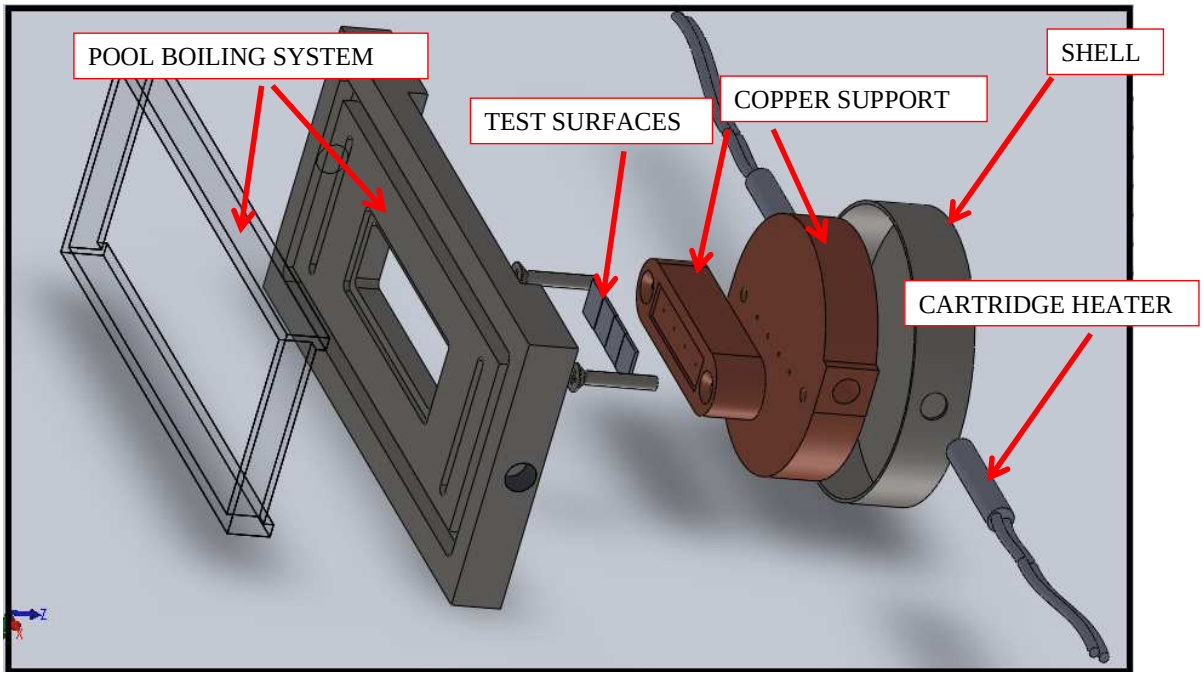

Figure 3. Global view of the test pool boiling section.

Type-K thermocouples are used to monitor and acquire the temperature along the copper block and at the heating surfaces (for practical reasons, related to the drawing interpretation, the location of all of the thermocouples is not shown here).

Methodology

Qualitative and quantitative characterization of the various pool boiling regimes is achieved by combining high-speed visualization with temperature measurements and heat transfer calculations. Different liquids are used, namely water, ethanol and methoxy-nonafluorobutane $C_4F_9OCH_3$ (HFE-7100) to infer on the effect of the liquid properties and of the various wetting regimes. Being a dielectric fluid, the nonafluorobutane $C_4F_9OCH_3$ (HFE-7100) is particularly interesting in the context of cooling applications for electronic devices. Furthermore, surfaces made of different materials, namely glass (bare and coated with an Indium Oxide film), aluminium, copper and silicon wafers are prepared to have various random and patterned topographies, to describe this effect on the bubble boiling dynamic mechanisms and consequently on the heat flux. The Nukiyama curve is reconstructed for the various liquids and surfaces, based on the visualization of the boiling morphology and on the heat flux calculations. A detailed analysis of the boiling mechanisms (*e.g.* bubble departure diameter and frequency, nucleation site densities) is performed by extensive image post-processing. The dynamic bubble boiling mechanisms are then associated with the heat flux measurements, to infer on the liquid/surface topography configuration which optimizes the heat flux, while keeping the boiling mechanisms controlled as desired.

Characterization of the surfaces

The surfaces were characterized by the topography and by the wettability. The surfaces are made from silicon wafers and are micro-textured with regular patterns of square pillars. Topography is quantified by the amplitude of the pillars *h*, by the fundamental wavelength λ_R (the pitch, i.e. the distance between consecutive pillars) and by the side of the cross section of the pillar *a*. These quantities are measured with a mechanical and with an optical profilemeter. The customized patterns are further checked by SEM/EDS analysis.

The wettability is quantified by the equilibrium contact angles which are measured using the Sessile Drop Method (at room temperatures, inside a thermostatted ambient chamber - Ramé-Hart Inc., USA, model 100-07-00). The contact angles, measured with water on each tested surface are depicted in Table 3. These are mean values obtained from at least eight measures taken at different regions of the surface. The time evolution of the average contact angles is obtained by curve fitting and the final values are determined by extrapolation. Complete wetting ($\theta_{eq} \approx 0^o$) is observed for all the surfaces when wetted by the ethanol droplets. The detailed procedure can be found in (*e.g.* Moita and Moreira [24]). Table 1 also depicts a global overview of the materials and micro-textures used in this study, as well as the contact angles measured with water at room temperatures. The dimensions *a*, *h* and λ_R are defined as shown in Figure 4.

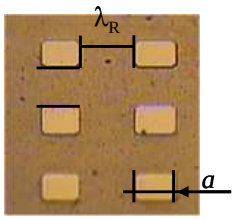

a)

Figure 4. Detail of a micro-textured surface showing the definition of the dimensions *a*, *h* and λ_R characterizing its topography.

Table 1. Summary of the main range of the topographical characteristics (as defined in Figure 4) used in the customized micro-textured surfaces. The rough asperities are square pillars with side of the cross section area *a*.

	a [μm]	*h* [μm]	λ_R [μm]
LISO (polished surface)	≈0	≈0	≈0
ARM1	85	1.2	230
ARM2	282	7.6	342
ARM3	224	13.5	446
ARM4	127	12.8	177

Results

The first results presented here were obtained using a glass surface, coated by the Indium Oxide film, as the heated well. These paragraphs are aimed at providing a global characterization of the pool boiling mechanisms for liquids with small surface tension, which completely wet the surface. In this context, Figure 5 depicts the Nukiyama curve of methoxy-nonafluorobutane $C_4F_9OCH_3$ (HFE-7100) in the test section with and area 5.25 cm^2.

The curve is obtained from seven individual tests. The collapse of all the experimental data confirms a good reproducibility of the results. It is worth noting that this plot only reconstructs part of the boiling curve, which is highlighted in Figure 6. The sequence of images depicted in Figure 5 identifies the morphological features observed within the different boiling regimes, thus allowing a "qualitative reconstruction" of the Nukiyama curve.

From the curve depicted in Figure 5 it is possible to identify the slope variation which is associated to the transition from the free convective region to the nucleate boiling region.

This slope variation is caused by the higher heat transfer coefficient which characterizes the nucleate boiling region and can be attributed to the effect of a vigorous convection in the liquid, coupled with the bubble formation itself. The qualitative characterization of the boiling process, presented in Figure 7, further contributes to understand the bubbles dynamics. So, as the heat flux increases, the isolated bubbles, which are observed at the insipient boiling, experience a fast grow and depart off the surface, activating a nucleation site, from which other bubbles are continuously formed. Further increasing the heat flux, the number of active nucleation sites also increases. The isolated bubbles start to merge, leading to the formation of jets and columns.

The evaluation of the heat flux is performed by both increasing and decreasing the heat flux. The curves obtained, which are shown in Figure 8, have some differences, namely because the incipient boiling and free convection regions are less extensive for the curve obtained by decreasing the heat flux. These differences are attributed to hysteresis phenomena, also reported by Mohamed and Bostanci [27]. The visualization of the boiling mechanisms also reveals that increasing the heat flux may favor the sudden transition in the boiling regimes, from a very incipient boiling to an explosive boiling, with the formation of jets and columns.

It is worth mentioning that sudden increase of the slope which characterizes the transition from the free convection region to the nucleate boiling region is quite small, contrarily to the curves shown in many studies reported in the literature (*e.g.* Mohamed and Bostanci [27]). This is attributed to the complete wetting behaviour of the liquid boiling over a very smooth surface (glass) with a very low effusivity. Similar behaviour is reported for instance in McHale and Garimella [26].

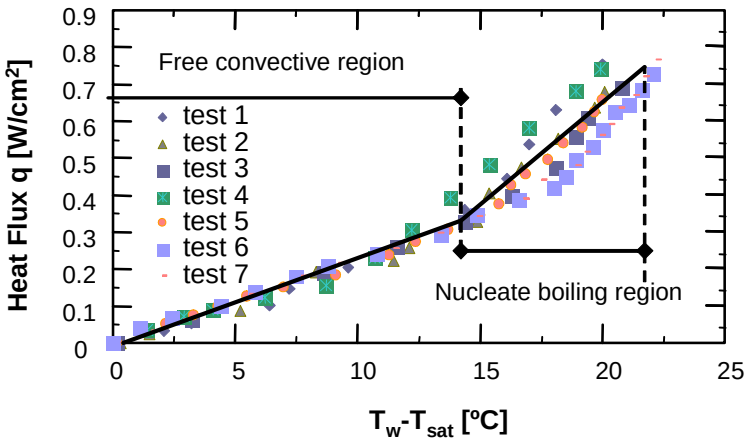

Figure 5. Reconstruction of the Nukiyama curve for HFE7100.

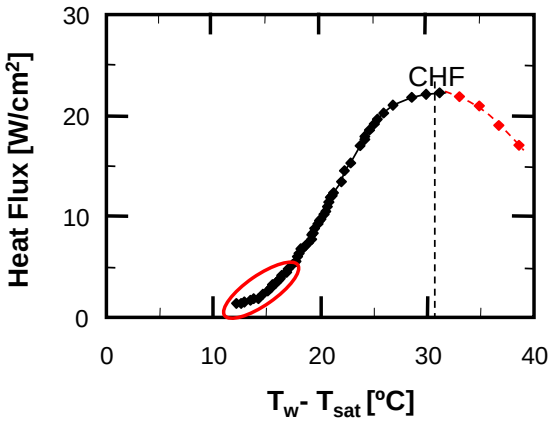

Figure 6. Overall view of the Nukiyama curve, represented up to the Critical Heat Flux. Adapted from Mohamed and Bostanci [27].

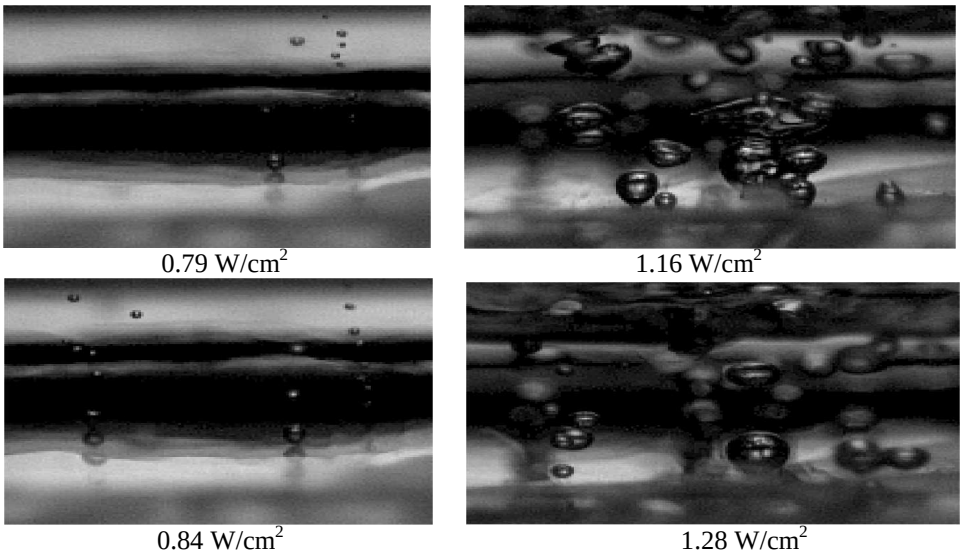

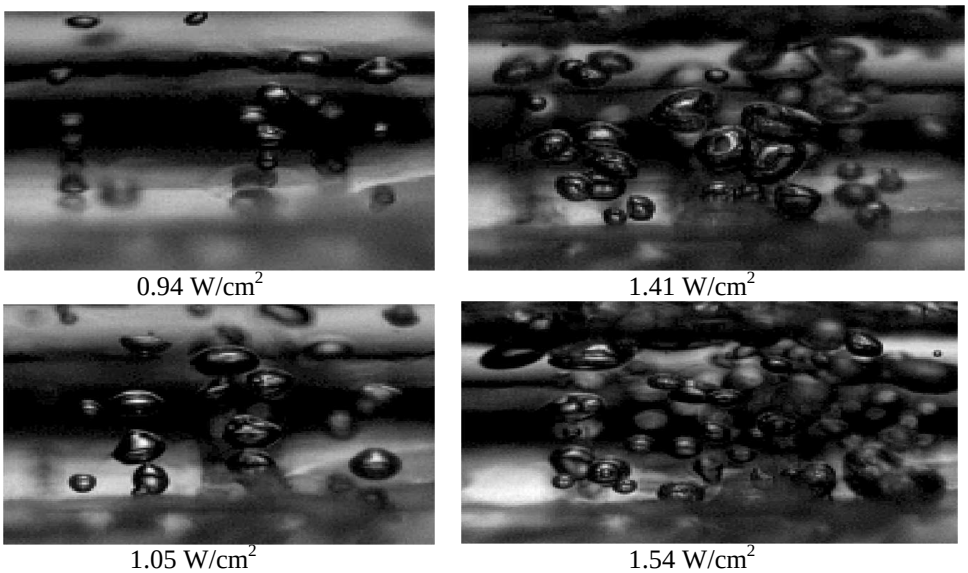

Figure 7. Qualitative characterization of the pool boiling process of HFE7100. The physical width of each image is approximately 20 mm.

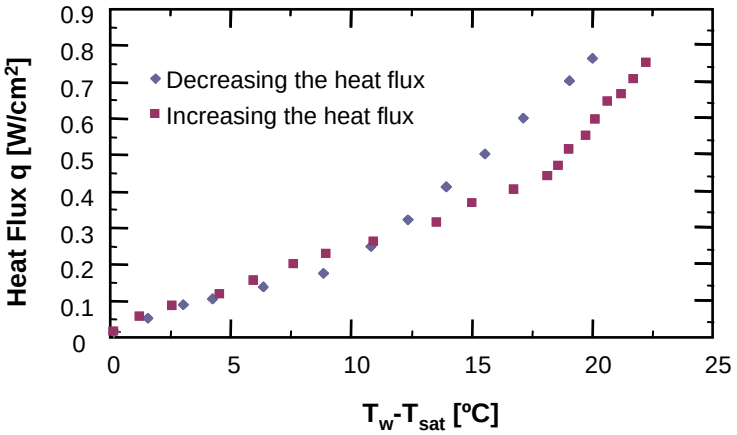

Figure 8. Comparison between the curves obtained by succeeding increasing or decreasing the heat flux.

Effect of the liquid properties

The results presented so far are obtained for liquids with small surface tension, which completely wet the surface. Under these conditions large superheat is required to initiate the nucleate boiling. Small increase of the surface tension and of the latent heat of evaporation completely alters the boiling morphology. This is clear by comparing the boiling morphology of HFE7100, depicted in Figure 7 with that of ethanol, in Figure 9, which has slightly larger surface tension (σ_{lv} HFE7100@20ºC=13.6x10^{-3}N/m; σ_{lv} ethanol@20ºC=22x10^{-3}N/m) and larger latent heat of evaporation ((h_{fg} HFE7100@20ºC=122.6KJ/KgKm; h_{fg} ethanol@20ºC=846KJ/KgK).

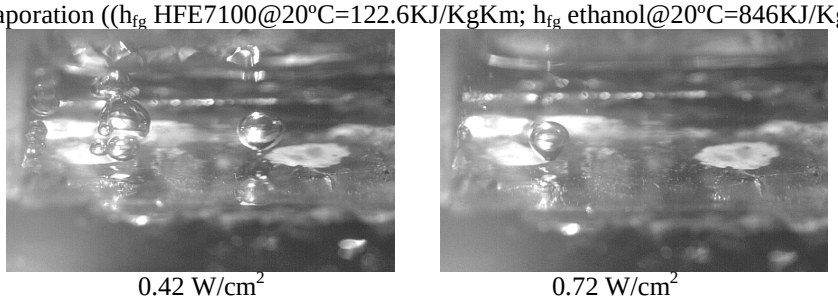

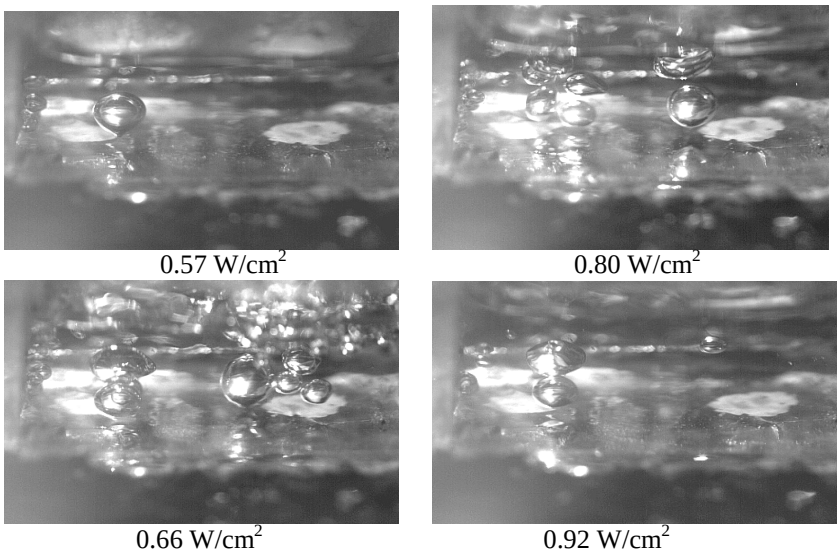

Figure 9. Qualitative characterization of the pool boiling process of ethanol. The physical width of each image is approximately 20 mm.

Ethanol presents a violent incipient boiling in which, compared to the HFE7100, generating larger and less distributed bubbles. Furthermore, the ethanol requires a higher superheat to reach the incipient boiling region, as depicted in Figure 10. Although both fluids are defined as well wetting liquids, the slightly higher value of σ_{lv} for ethanol is enough to delay the boiling process and to cause the non-uniformity of the nucleation sites distribution, when compared to HFE7100. However, once h_{fg} is overcome, an "explosive boiling" occurs. This non-uniform boiling behaviour seems to deteriorate the efficiency of the pool boiling heat transfer for ethanol.

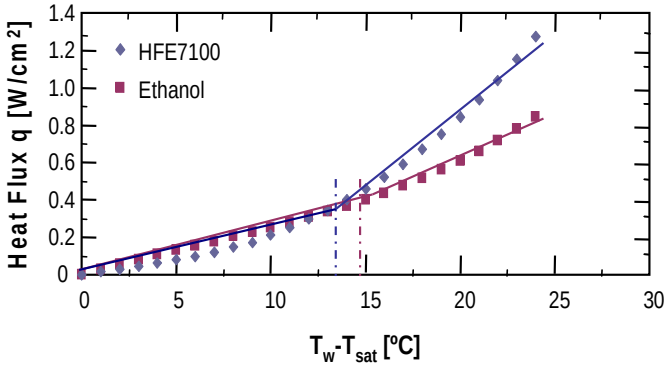

Figure 10. Comparison between HFE7100 and ethanol boiling curves. In both cases, the vertical dot lines highlight the transition from the free convention region to the nucleate boiling region

A more detailed characterization of the boiling process of the two liquids can be provided by analyzing the boiling morphology and bubble dynamics, as discussed in the following paragraphs. This analysis is based on the evaluation of some of the most characteristic parameters that describe the bubble nucleation characteristics in pool boiling, namely the departure diameter D_d the departure frequency f_d, the product f*Dd and the cumulative active nucleation site density N/A. The bubble departure diameter, the active nucleation sites density and the departure frequency are compared in Figure 11 for HFE7100 and ethanol.

The bubble departure diameter for HFE 7100 was observed to increase with the Jacob number and therefore with the heat flux. The results are in agreement with those reported by McHale and Garimella [26], particularly at low heat fluxes, comparable to those considered in this part of the study. They are also in fairly good agreement with the correlations of Mohamed and Bostanci [27] and of Cole [28], also for low heat fluxes. This trend can be explained as in Zuber [29]: for very low wall superheat the bubble departure is solely a function of the buoyancy and of the surface tension. As the surface temperature increases, the surface tension decreases (for most fluids), which should result in the decrease of the departure diameter. However, as the superheat increases, dynamic forces (i.e. inertial forces) start dominating the bubble growth process and hence the bubble diameter increases with the surface temperature. A different trend is however observed in ethanol which presents a sharp increase of the bubble departure diameter at low heat fluxes, but starts to decrease at higher heat fluxes. This trend shows a discrete match with the results reported by McHale and Garimella [26].

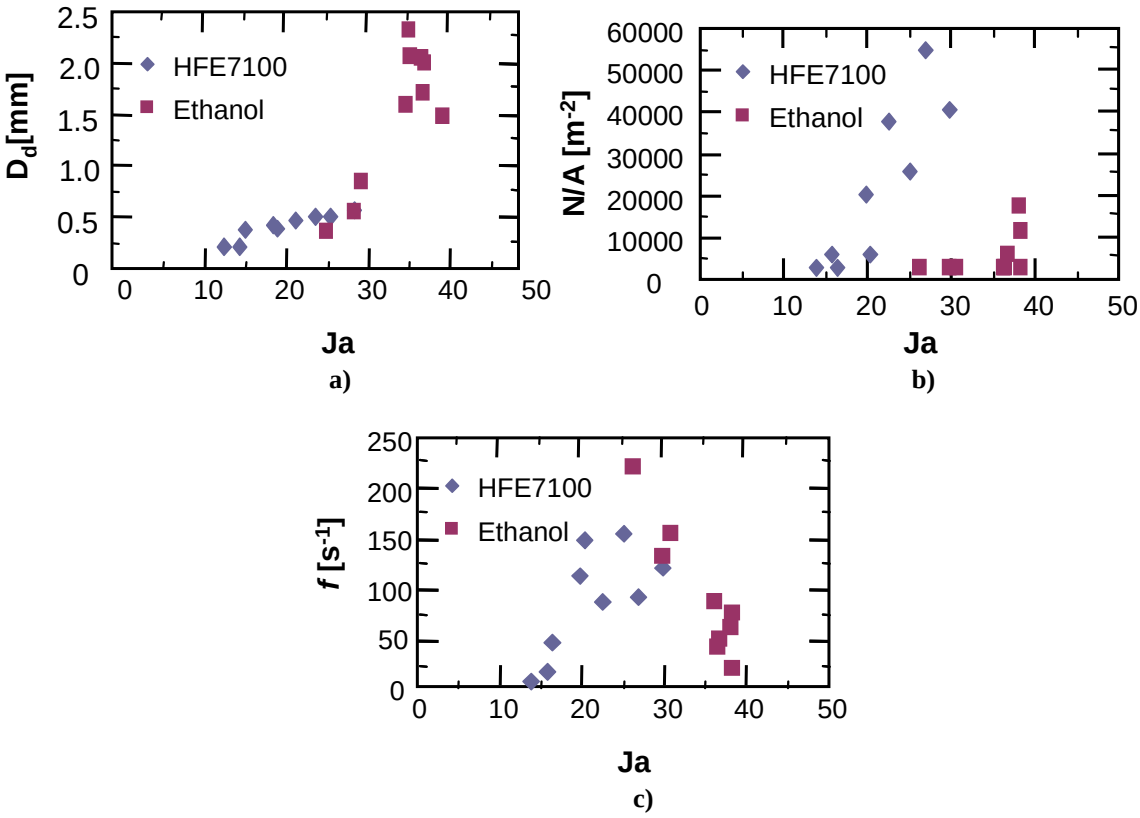

Figure 11. Comparison of the bubble morphology for HFE7100 and ethanol. a) departure diameter, b) active nucleation sites density and c) departure frequency.

The departure frequency for HFE 7100 presents a particular behavior, showing a sharp increase for lower heat flux. However, at higher heat fluxes, and therefore larger bubble departure diameters, the frequency should decrease, but instead, seems to oscillate around an average value of 117.75 Hz. The more distributed boiling of HFE 7100 can explain this behaviour. Hence, given that the departure diameters presented here are averaged sizes, when the heat flux increases, larger bubbles are produced, but yet, small bubbles still departure for a large number of active nucleation sites. Consequently, the averaged departure size of the bubbles can be larger, but the corresponding averaged departure frequency may result in this oscillatory behaviour. A similar trend is reported by Ramaswamy *et al.*[29], at low and similar values of heat fluxes, who attributed this behaviour to the small dimensions of the pool size. In the present work, the effect of the size of the pool was investigated and any significant differences were observed in the boiling curves. However, there may be indeed some influence of the dimensions of the pool in the observed bubble dynamics.

A completely different trend is again observed for ethanol. In fact, in this case the departure frequency has been found to decrease monotonically within the entire range of heat fluxes evaluated. This is due to the "explosive boiling" of the ethanol at the very early stages of nucleation. Afterwards, the process stabilizes leading to the formation of bigger bubbles, with consequent lower departure frequency.

Finally, the nucleation sites density is observed to increase with the surface superheat for both HFE7100 and ethanol, as expected. These values are smaller than those reported in the literature, which is attributed to the use of very well wetting liquids on a very smooth heating wall, with low effusivity, as previously explained.

Main differences between these two liquids can be summarized as follows: ethanol requires a higher superheat (higher Jacob) to reach the incipient boiling region which is related to the more violent bubbles formation with average bigger departure diameters. The surface tension has a vital role in the phenomena described above so that the slightly larger surface tension of ethanol is partially responsible for the reported dissimilar behaviour, namely for the sparser active nucleation sites and globally larger departure bubble diameter. The larger σ_{lv} should promote the nucleate boiling regime to occur for lower wall superheat. However in the present case, the use of an extremely smooth surface will lessen this mechanism since "rough cavities" are almost inexistent and the liquid used wets the surface completely. Therefore, the increase of the surface tension may actually be acting in the opposite way, further delaying the transition from the free convection region to the nucleate boiling region for higher wall superheat. Additionally, the fact that the latent heat of evaporation of ethanol is about seven times larger than that of HFE7100 further contributes to increase the wall superheat required to trigger the incipient boiling

Effect of surface topography

In this sub-section, the influence of surface topography on the pool boiling process is experimentally investigated over a wide range of roughness values, gathered in three representative micro-textured surfaces. Water, ethanol and HFE 7100 are used to consider the significantly different surface tension values which will affect the wetting behaviour. The analysis considers the effect of surface topography on the heat transfer and how it is related to the boiling morphology. For this part of the work, the textured surfaces are accommodated on a copper block heated by electrical cartridge heaters, using the experimental apparatus schematically represented in Figure 2 and 3.

The boiling curves and the heat transfer coefficient for water pool boiling are represented in Figure 12. The Figure shows that the lowest superheat required to trigger the incipient nucleate boiling is achieved with the surface having the higher pillars, while the lowest superheat at a given heat flux is obtained for the smoothest surface. Consistently, the surface with the largest pillars/cavities shows approximately a 166% improvement in the heat transfer coefficient compared to the smoothest. Considering the ratio between the high of the pillars and the distance between them, h/λ_R as suggested in Moita and Moreira [24], the heat transfer coefficient is smaller for decreasing values of h/λ_R.

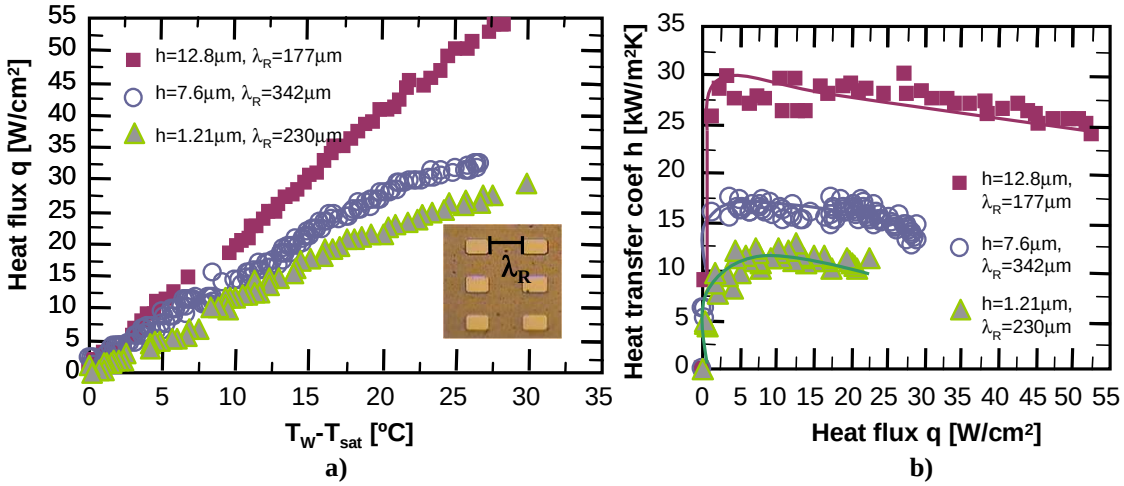

Figure 11. Effect of the micro-textures in a) heat flux *vs*. wall superheat, b) heat transfer coefficient for pool boiling of water.

A similar trend is observed for HFE7100 and ethanol.

These results are in disagreement with many studies reported in the literature (*e.g.* Grigoriev [30]), which report that once a surface is sufficiently rough, there is no benefit to additional roughening. However, they are consistent with recent investigations presented by Jones *et al.* [25] who show that an improvement in the heat transfer coefficient can be achieved when increasing the scale of the cavities ten times (from 1 to 10µm), as long as these scales interfere with bubble dynamics. It is worth noting that both the depth of the cavities and the distance between affect these mechanisms. In this context one may observe a significant decrease in the heat transfer coefficient for very high heat fluxes of water boiling, which is not so evident for HFE7100. This is related to the higher surface tension of the water which, contrarily to HFE7100 will not completely enter into the rough cavities. Consequently, the visualization of water boiling on these surfaces, as illustrated inn Figure 12, shows bubble spreading over the surface and coalescing with bubble formed at other sites, which results in a larger area of the surface to entrap a vapor blanket, which will act as an insulator, thus leading to the decrease of the heat transfer coefficient.

Given this particular behaviour of the water, a more detailed boiling morphology is presented in the following paragraphs. Then, for reasons related to the limitations in the length of the paper, only a summarized comparison is briefly discussed between the water, HFE7100 and ethanol. Water boiling is characterized by a strong coalescence, for almost all the test surfaces analyzed. The interaction between adjacent bubbles is so evident that lead to a difficult evaluation of the real dimension of the diameter of the bubble at the departure and of the value of active nucleation sites. Although the heat transfer seems to be enhanced for the surfaces with the surface having the higher amplitudes, it should be mentioned that the ratio h/λ_R increases for these surfaces at the expense of playing with the distance between the peaks. Therefore looking at Figure 13, it is not so obvious that increasing h or increasing h/λ_R will lead to larger departure diameters or higher activate nucleation site densities. In fact, the value of D_d appears to be globally higher for the "less roughened surface" while for the other two test surfaces, D_d gradually increases with h.

s

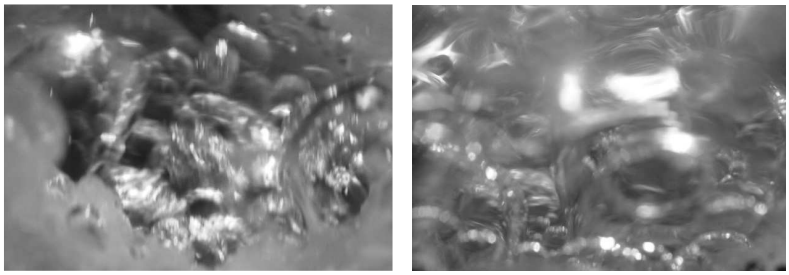

a) b)

Figure 12. Particular observation of the coalescence among bubbles for boiling water. The physical width of each image is approximately 8 mm. a) q= 51.75 W/cm^2 surface h=12.8μm, λ_R=177μm, ΔT=22.98; b) q=28.20 W/cm^2, surface h=1.21μm, λ_R =230μm, ΔT=22.57ºC.

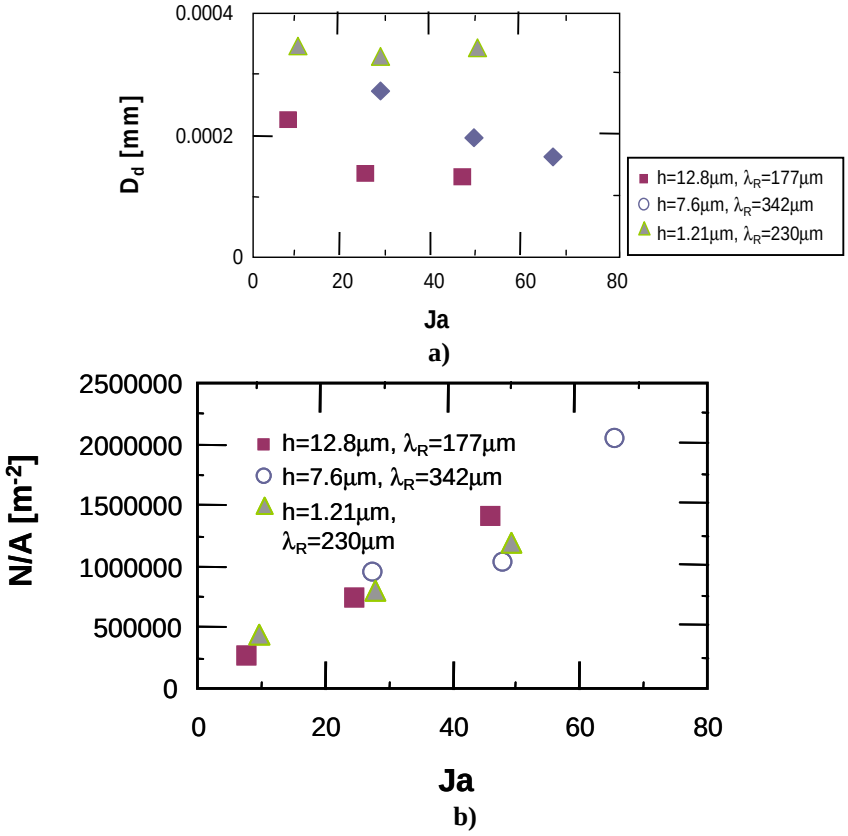

Figure 13. Effect of surface topography on bubble morphology of water. a) departure diameter, b) active nucleation sites density.

Additionally, there is no significant difference in the trend of the active nucleation sites within the various surfaces. Therefore, it is worth to perform a more detailed analysis for gradually larger heat fluxes (and therefore larger values of the Jakob number, Ja)

8 <Ja< 10

Within this range of heat flux, it was only possible to compare the surface with lower h/λ_R and the surface wit intermediate value. The visualization of bubble morphology is illustrated in Figure 14.

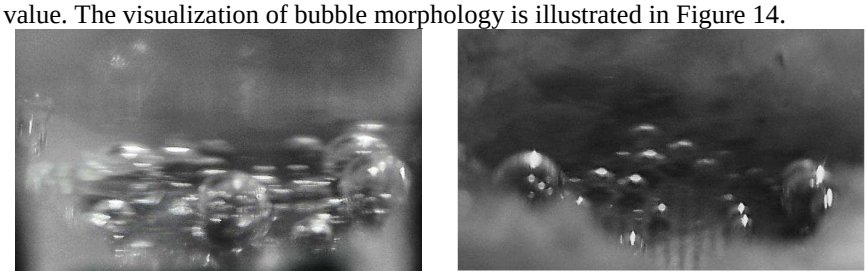

a) h=12.8μm, λ_R=177μm, Ja = 9.82 **b)** h=7.6μm, λ_R=342μm, Ja = 7.9

Figure 14. Comparison between boiling morphology for water at 7.9<Ja<9.82 over different micro-textured surfaces. The physical width of each image is approximately 8 mm.

The surface with smaller *h* also has the smaller λ_R and the pillars have the smallest length *a*. The roughness amplitude h is high enough to promote nucleation but then, the cavities are also close enough to allow stronger coalescence.

24.73<Ja<28

In this range of Ja, as observed in Figure 15, the pool boiling of the water is similar for the three surfaces, resultingg in an almost equal value of active nucleation sites. Also here, the difference between *h* for the various surfaces is not high enough to promote significantly different boiling behaviour, so again coalescence is still promoted to smaller λ_R and therefore larger vapor bubbles appear within the surface with larger *h* (and smaller λ_R) and with the surface with smaller *h* (and small λ_R).

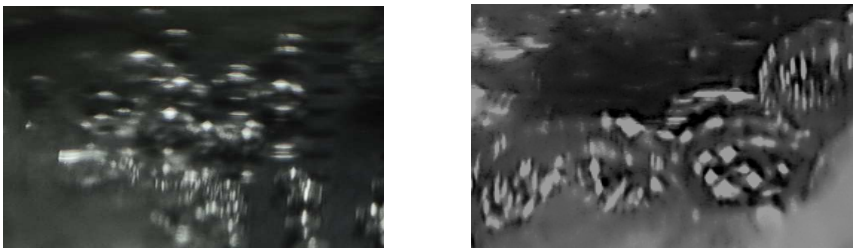

a) h=12.8μm, λ_R=177μm, Ja = 27.70 **b)** h=7.6μm, λ_R=342μm, Ja = 24.73

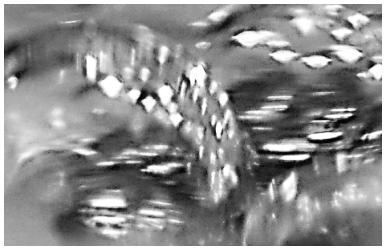

c) h=1.21μm, λ_R =230μm, Ja = 28.00

Figure 15. Comparison between boiling morphology for water at 24.73<Ja<28.00 over different micro-textured surfaces. The physical width of each image is approximately 8 mm.

46.03<Ja<49.09

Reaching the highest heat fluxes (Figure 16), the higher amplitude of the rough peaks is still enhancing formation of active nucleation sites, but then, *h* seems now to play an important role. In fact, within this range of Ja, the surface with higher pillars generates slightly higher value of active nucleation sites, although it is clearly not enough to evidence a dominant effect of the high of the rough pillars, when compared to the spacing between them.

a) h=12.8μm, λ_R=177μm, Ja = 48.79

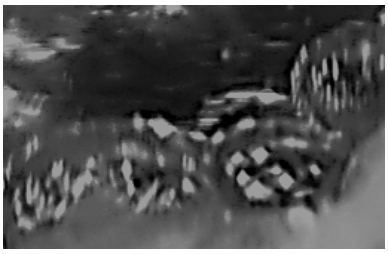

b) h=7.6μm, λ_R=342μm, Ja =46.03

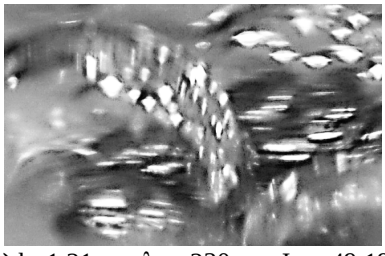

c) h=1.21μm, λ_R =230μm, Ja = 49.19

Figure 16. Comparison between boiling morphology for water at 46.03<Ja<49.19 over different micro-textured surfaces. The physical width of each image is approximately 8 mm.

Ja=65.66

For this value of Jackob only the surface h=12.8μm, λ_R=177μm has been studied. The figure shows an example of the vapor entrapment: small vapor bubbles are formed and keep entrapped within the rough pillars. The heat flux in this case is now high enough to generate large bubbles which will coalescence forming a huge vapor bubble that does not depart from the surface, acting as an insulator vapor blanket. This mechanism is highlighted in Figure 17.

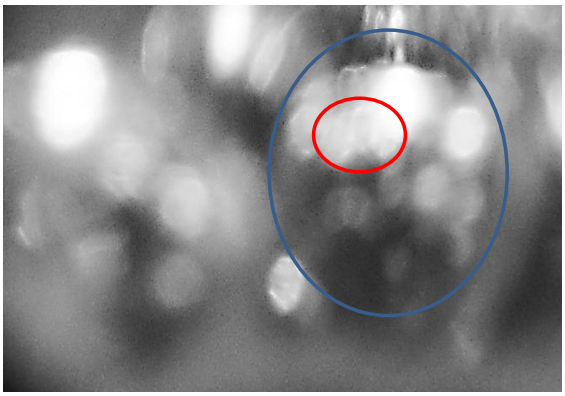

Figure 17. Between boiling morphology for water on the structured surface h=12.8μm, λ_R=177μm, Ja=65.66 over different micro-textured surfaces. The physical width of each image is approximately 8 mm.

Combined effect of wettability and surface topography

The discussion presented up to now leads to the unequivocal argument that the overall cooling performance of pool boiling depends on the wettability and on the surface topography, not only the roughness amplitude but also the distance between the rough peaks, which affect the boiling morphology and the bubble dynamics. For illustration purposes, Figure 18 depicts the boiling curve and the heat transfer coefficient of water, ethanol and HFE7100 on the rough surface *h*=12.8μm, λ_R=177μm.

Water resulted in the lowest superheat at a given heat flux, while HFE 7100 was associated to the highest superheat. Additionally, water was associated to the highest value of heat transfer coefficient while HFE 7100 to the lowest. However it should be noticed that while for water and ethanol the slope of the curve is decreasing at higher heat fluxes, thus resulting in a decrement of the heat transfer coefficient, for HFE 7100 instead, the value of the heat transfer coefficient has been found to continuously increase. This is attributed to the dissimilar wet-

ting effects of the liquids. So, while for the water the high surface tension promotes the vapor blanket entrapment, such phenomenon is not likely to occur with HFE7100, so that for higher heat fluxes HFE 7100 may actually provide a better cooling performance. The critical value of h/λ_R should be therefore related to the ratio between the departure diameter D_d and the spacing λ_R (the ratio D_d/λ_R is suggested by Nitesh *et al*. [17], who however do not account for the effect of the roughness amplitude, that seems to be non-negligible in many studies reported in the literature and also in the present work) as well as to the size of the bubbles resulting from coalescence inside each rough cavity.

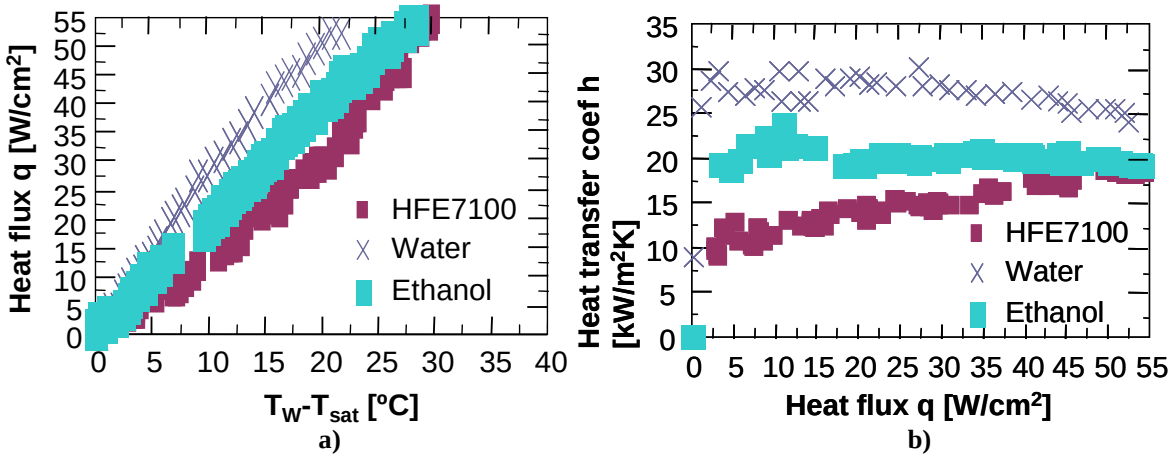

Figure 18. Boiling curves of water, ethanol and HFE7100 on the surface h=12.8μm, λ_R=177μm. a) heat flux versus wall superheat, b) heat transfer coefficient versus heat flux.

Final remarks

The present work considers the detailed analysis of the physical processes involved in pool boiling, in the context of micro-cooling applications. The results clearly show the strong effect of wettability and of the surface topography on the boiling morphology, and consequently on the heat transfer mechanisms. Hence, liquids with low surface tension will completely wet all the surfaces, delaying the triggering of nucleation. For these wetting conditions, increasing the latent heat of evaporation will require larger superheat to enter into the incipient boiling region, regardless the surface topography. Also, small increase of the surface tension and/or of the latent heat of evaporation leads to significantly different bubble dynamics. An enhancement of the heat transfer is achieved with micro-textured surfaces, within the roughness scales used here, by controlling the bubble dynamics with the rough cavities. For partially wetting liquids, having larger surface tension (*e.g.* water) the relation between the roughness amplitude *h* and the distance between the cavities λ_R has a strong effect in the coalescence of vapor bubbles, so that critical ratios h/λ_R promote the entrapment of a vapor blanket, which acts as an insulator, leading to the decrease of the heat transfer coefficient. This is extremely important in the design of smart interfaces for spray cooling and particularly in micro-channels, for which the uncontrolled formation of vapor pockets may quickly lead to clogging problems. Also, the heat transfer coefficient associated to these vapor blankets is known to lead to burnout scenarios of the systems cooled with microchannels.

Acknowledgments

The authors acknowledge the contribution of Fundação para a Cência e a Tecnologia (FCT) by supporting A. S. Moita with a Fellowship (Ref:SFRH/BPD/63788/2009).

The authors are also grateful to FCT for partially financing the research under the framework of project PTDC/EME-MFE/109933/2009 and for supporting E. Teodori with a research grant.

References

[1] ITRS, International Technology Roadmap for Semiconductors, (2006).
[2] Mudawar, I., *IEEE Transaction on Components and Packaging*, 124 (2):122-141 (2001).
[3] Lord Rayleigh, Philosophical Magazine, 34:94-98 (1917).
[4] Nukiyama, S., *J. Soc. Mech. Eng.. Japan*, 37(6):367-374 (1934). Translated by Lee, C. J. in the *Int. J. Heat Mass Transf.*, 9:1419-1433 (1966).
[5] Jakob, M., *Am. Soc. Mech. Eng.*, 58:643–660 (1936).
[6] Westwater, J. W., *Am. Sci.*, 47:427–446 (1958).
[7] Clark, H. B., Strenge, P. S., and Westwater, J. W., *Chem. Eng. Prog., Symp. Ser.*, 55(29):103–110 (1959).
[8] Bankoff, S. G., *Trans. ASME*, 79:735–740 (1958).
[9] Griffith, P., and Wallis, J. D., *Chem. Eng. Prog., Symp. Ser.*, 56(30):49–63 (1960).

[10]Hsu, Y. Y., *ASME J. Heat Transfer*, 84:207–216 (1962).
[11]Corty, C., Foust, A. S., *Chem. Eng. Prog., Symp. Ser.*, 51(7):1–12 (1955).
[12]Kurihara, H. M., and Myers, J. E., *AIChE J.*, 6(1):83–91 (1960).
[13]Hsu, S. T., Schmidt, F. W., *ASME J. Heat Transfer*, 83:254–260 (1961).
[14]Marto, P. J., Rohsenow, W. M., *ASME J. Heat Transfer*, 88:196–204 (196).
[15]Berenson, P. J., *Int. J. Heat Mass Transfer*, 5:985–999 (1962).
[16]Chih Kuang Yu, Ding Chong Lu, Tsung Chieh Cheng, *J. Micromechanics and Microengineering*, 16:2092-2099 (2006)~.
[17]Nitesh D., Nimkar,Sushil H.Nhavnai , Richard C.Jaeger, *Int. J. Heat and Mass Transf.*, 49:2829-2839 (2006).
[18]Hutter, C., Kenning, D.B.R., Sefiane , K., Karayiannis, T. G., Cummins, H. Lin , G., Walton , A. J., *Exp. Thermal Fluid Science*, 34:422-433 (2010).
[19]Dhir, Vijay K. , Abarajith, Hari S., Li, Ding, *Heat Transfer Engineering*, 28(7): 608-624 (2007).
[20]Zhang, L., Shoji, M., *Int. J. Heat and Mass Transf.*, 46:513–522 (2003).
[21]Lee, H.C., Oh, B.D., Bae, S.W., Kim, M.H., *Int. J. Multiphase Flow*, 29:1857–1874 (2003).
[22]Kim, J., Oh, B.D., Kim, M.H., *Int. J. Multiphase Flow*, 32:208–231 (2006).
[23]Luke, A., In: Proceedings of 5th international conference on boiling heat transfer, 20030504-08 (2003).
[24]Moita, A. S., Moreira, Al. L. N., *Exp. Fluids*, doi: 10.1007/s00348-011-1106-2, Available online (2011).
[25]Jones, B. J., McHale, J. P., Garimella, S. V., *J. Heat Transfer*, 131:121009-1-14 (2009).
[26]McHale, J. P., Garimella, S. V., *Int. J. Multiphase Flow*, 36:249-260 (2010).
[27]EL-Genk , M., Bostanci, H., Int. J. Heat and Mass Transf., 46:1841–1854 (2003).
[28]Cole, R., *AIChE Journal*, 13(4) :779–783 (1967).
[29]Ramaswamy C, Joshi Y, Nakayama W, Johnson W.B. , Int. J. Heat Mass Transf., 45:4761–4771 (2002).